


# Numerical modeling of space-time wave extremes using WAVEWATCH III

Francesco Barbariol<sup>1</sup>  · Jose-Henrique G. M. Alves<sup>2</sup> · Alvise Benetazzo<sup>1</sup> · Filippo Bergamasco<sup>4</sup> · Luciana Bertotti<sup>1</sup> · Sandro Carniel<sup>1</sup> · Luigi Cavaleri<sup>1</sup> · Yung Y. Chao<sup>3</sup> · Arun Chawla<sup>3</sup> · Antonio Ricchi<sup>5</sup> · Mauro Sclavo<sup>1</sup> · Hendrik Tolman<sup>3</sup>

Received: 17 March 2016 / Accepted: 30 November 2016 / Published online: 23 January 2017  
© Springer-Verlag Berlin Heidelberg (outside the USA) 2017

**Abstract** A novel implementation of parameters estimating the space-time wave extremes within the spectral wave model WAVEWATCH III (WW3) is presented. The new output parameters, available in WW3 version 5.16, rely on the theoretical model of Fedele (J Phys Oceanogr 42(9):1601–1615, 2012) extended by Benetazzo et al. (J Phys Oceanogr 45(9):2261–2275, 2015) to estimate the maximum second-order nonlinear crest height over a given space-time region. In order to assess the wave height associated to the maximum crest height and the maximum wave height (generally different in a broad-band stormy sea state), the linear quasi-determinism theory of Boccotti (2000) is considered. The new WW3 implementation is tested by simulating sea states and space-time extremes over the Mediterranean Sea (forced by the wind fields produced by the COSMO-ME

atmospheric model). Model simulations are compared to space-time wave maxima observed on March 10th, 2014, in the northern Adriatic Sea (Italy), by a stereo camera system installed on-board the “Acqua Alta” oceanographic tower. Results show that modeled space-time extremes are in general agreement with observations. Differences are mostly ascribed to the accuracy of the wind forcing and, to a lesser extent, to the approximations introduced in the space-time extremes parameterizations. Model estimates are expected to be even more accurate over areas larger than the mean wavelength (for instance, the model grid size).

**Keywords** Space-time wave extremes · WAVEWATCH III · Ocean waves · Stereo vision · Numerical modeling

---

This article is part of the Topical Collection on the *14th International Workshop on Wave Hindcasting and Forecasting in Key West, Florida, USA, November 8–13, 2015*

---

Responsible Editor: Oyvind Breivik

✉ Francesco Barbariol  
francesco.barbariol@ve.ismar.cnr.it

- <sup>1</sup> Institute of Marine Sciences, Italian National Research Council (ISMAR-CNR), Venice, Italy
- <sup>2</sup> Systems Research Group Inc. at Marine Modeling and Analysis Branch, Environmental Modeling Center, NCEP/NOAA, College Park, MD, USA
- <sup>3</sup> Marine Modeling and Analysis Branch, Environmental Modeling Center, NCEP/NOAA, College Park, MD, USA
- <sup>4</sup> Ca' Foscari University of Venice, Venice, Italy
- <sup>5</sup> Università Politecnica delle Marche, Ancona, Italy

## 1 Introduction

Reliable prediction of ocean wave extremes has always been foremost for off-shore platform design, coastal activities, and navigation. Indeed, many severe accidents and casualties at sea have been most likely ascribed to abnormal and unexpected waves (Kharif and Pelinovsky 2003; Didenkulova et al. 2006). However, predicting wave extremes is a challenging task, because the mechanisms that lead to their formation are still far from being completely understood. Moreover, the observation of ocean waves, of primary importance to verify theoretical models, is limited by the costs and risks of deployments during severe open-ocean sea-state conditions. As a consequence, in many cases, the theoretical and modeling frameworks used to estimate wave maxima have been ineffective in warning seafarers or avoiding structural damage to offshore facilities (Forristall 2006, 2007). In this context, significant efforts are being undertaken to better understand wave

extremes (e.g., Onorato et al. (2001); Janssen (2003); Dysthe et al. (2008); Gemmrich and Garrett (2008); Cavaleri et al. (2016a, 2016b); Fedele (2015)) even if up to now research has not yet provided a more complete framework to explain the occurrence of extremely large waves (i.e., waves that are outlier for standard wave statistics) in realistic sea conditions.

Traditionally, the observations that served to verify statistical wave models have relied on single-point measuring systems (e.g., buoys, gauges). Recent observations of short-crested waves, capable of capturing the full space-time evolution of wave groups, have shown that the extreme crest height attained over a sea surface area can be significantly larger than when measured at a single point (e.g., Fedele et al. (2013) and Benetazzo et al. (2015)). The same evidence has also been verified with numerical simulations (e.g., Socquet-Juglard et al. (2005); Forristall (2006); and Barbariol et al. (2015)), and indirectly pointed out by the frequent damage caused by stormy waves to off-shore facilities, at elevations considerably higher than those regarded to be safe by virtue of design extreme wave models and engineering safety factors (Forristall 2007). This suggests that structures having a wider-than-point footprint on the ocean may be subject to larger waves than those typically observed by single-point instruments, and predicted by corresponding statistical models (Forristall 2006).

In this context, more recent scientific effort has been devoted to the development of a theoretical wave modeling framework that could lead to the prediction of the so-called “space-time extremes” (STE), i.e., the highest crest and wave heights occurring during a sea state of given duration and over a given sea area (Fedele 2012). Relying on recent developments in the analysis of multidimensional random fields maxima (Adler and Taylor 2007; Piterbarg 1996), a model for STE wave crests based on the “Adler and Taylor Euler Characteristics approach” was first proposed by Fedele (2012). It was extended to account for second-order nonlinearities by Benetazzo et al. (2015), and verified by Barbariol et al. (2014), Benetazzo et al. (2015) and Fedele et al. (2013) with actual sea-state observations. Recently, a state-of-the-art third-order nonlinear model has been formulated by Fedele (2015). In addition, a modeling framework for maximal wave heights is provided by the quasi-determinism theory (QD, Boccotti (2000)) which relates large wave and crest heights of space-time wave groups. In this context, Benetazzo et al. (2016, Space-time extreme wind waves: analysis and prediction of shape and height, unpublished; supported by real-sea observations) coupled STE model results with QD theory in order to predict shape and height of high waves.

For oceanographic applications, STE prediction is shown to rely on the directional wave spectrum that provides,

through integral parameters, some geometric and kinematic features of the sea state (Baxevani and Rychlik 2006). Thus, spectral wave forecasting models, typically employed for hindcasts and forecasts of sea states, are promising candidates for providing directional wave spectra that may produce large-scale predictions of STE. Barbariol et al. (2014) have shown that STE hindcasts can be performed at large scales using the third-generation spectral wave model SWAN (Booij et al. 1999), which was adapted to provide integral spectral parameters used to compute STE, allowing preliminary tests over the Italian seas to be performed by Sclavo et al. (2015).

In this study, we combine theoretical, experimental, and numerical modeling approaches to show that, using numerical model outputs, estimates of STE crest and wave heights can be obtained. To this end, we have implemented the second-order nonlinear model for STE wave crests (Fedele 2012; Benetazzo et al. 2015), and the linear model for STE wave heights (Boccotti 2000; Fedele 2012) within the state-of-the-art WAVEWATCH III (WW3) spectral wave model (Tolman 1991; WW3DG 2016). An assessment of the capabilities of the novel implementation is described, whereby WW3 simulations on the Mediterranean Sea forced with winds from the COSMO-ME (Steppeler et al. 2003) atmospheric model, are compared to STE observed in March 2014, during a wave acquisition stereo system (WASS, Benetazzo et al. (2012)) experiment at the ISMAR-CNR “Acqua Alta” oceanographic tower (Fig. 1), in the northern Adriatic Sea (Italy).

We start the paper introducing the theoretical framework adopted to model the STE, and showing the results of the stereo experiment at “Acqua Alta” (Section 2). Next, in Section 3, we direct our focus to the numerical modeling, describing the implementation procedures. In Section 4, we present the test case where we have compared modeled spectra and STE to observations at “Acqua Alta,” and in Section 5, we close the paper with a discussion of wave model and STE parameter estimation skills.

## 2 Space-time extremes of ocean waves

In this section, the most relevant features of sea-state STE are briefly presented, focusing on theoretical modeling and observations that are functional to the study. More in-depth descriptions are found in citations provided in this section below, and in Section 1 above.

To estimate STE, we draw upon the model of Fedele (2012), which is based on the Euler characteristics approach by Adler (1981) and Adler and Taylor (2007). In brief, that model states that in a multidimensional, homogeneous, and stationary Gaussian random field, the probability of

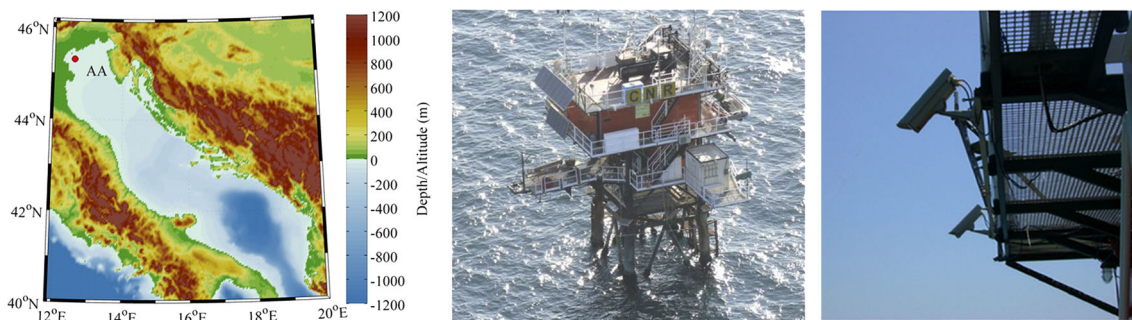


**Fig. 1** The “Acqua Alta” oceanographic tower (*middle*) in the northern Adriatic Sea (*left*), and the WASS stereo-photogrammetric system (*right*) mounted on the rooftop

exceedence of its extreme values can be estimated by means of the Euler characteristic of the excursion set (i.e., the subsample of the field exceeding the threshold), provided the threshold is high compared to the standard deviation of the field. In the context of ocean waves, the random field is the sea surface elevation  $\eta(x, y, t)$ , which is function of time  $t$  and of the two-dimensional space  $(x, y)$ . Thus, if the space-time domain is large enough to capture the full evolution of a wave group, the Fedele (2012) model provides the exceedence distribution function for the highest linear crests in the domain.

Herein, we account for the nonlinear second-order extension of the Fedele (2012) model proposed by Benetazzo et al. (2015) to evaluate the expected STE crest height. The wave height (crest-to-through) associated to the STE crest and the STE wave height stem from the quasi-determinism (QD) theory of Boccotti (2000), in its linear version—in this study, we do not account for second-order nonlinear effects on wave heights, as the contribution they add is rather small compared to the linear part, both in narrow- and broad-band sea states. As a matter of fact, Benetazzo et al. (2016, Space-time extreme wind waves: analysis and prediction of shape and height, unpublished) showed that the linear QD theory and the linear Fedele model provide a good estimate of the observed maximum wave height over a space-time domain, whereas the second-order contribution is only a few percent of the linear estimate (see also Tayfun and Fedele (2007)). Moreover, computing second-order interaction kernels within a spectral wave model would likely require a huge computational effort, not compatible with the requirements of a forecasting model.

For the present study, estimates of wave STE were validated against reference observations gathered during a recent stereo-photogrammetric experiment (Benetazzo et al. 2015) at the “Acqua Alta” oceanographic tower (Italy), where STE have been observed and analyzed in the light of the theoretical modeling framework described next.

### 2.1 Theoretical framework

For the implementation in WW3, STE are defined in terms of the moments  $m_{ijl}$  of the directional wavenumber spectrum  $S(k, \theta)$

$$m_{ijl} = \int k_x^i k_y^j \omega^l S(k, \theta) dk d\theta \tag{1}$$

( $\omega$  being the angular wave frequency,  $k_x$  and  $k_y$  the components of the wavenumber  $k$  associated to  $\omega$ , and  $\theta$  the wave direction), and of the derived integral spectral parameters (Baxevani and Rychlik 2006; Fedele 2012)

$$\begin{aligned} T_m &= 2\pi \sqrt{\frac{m_{000}}{m_{002}}} & L_x &= 2\pi \sqrt{\frac{m_{000}}{m_{200}}} \\ L_y &= 2\pi \sqrt{\frac{m_{000}}{m_{020}}} & \alpha_{xt} &= \frac{m_{101}}{\sqrt{m_{200}m_{002}}} \\ \alpha_{yt} &= \frac{m_{011}}{\sqrt{m_{020}m_{002}}} & \alpha_{xy} &= \frac{m_{110}}{\sqrt{m_{200}m_{020}}} \end{aligned} \tag{2}$$

Here,  $T_m$  is the zero-crossing mean wave period,  $L_x$  is the mean wavelength (along the mean direction of wave propagation),  $L_y$  is the mean wave crest length (orthogonal to the mean direction of wave propagation), and  $\alpha_{xt}$ ,  $\alpha_{yt}$ ,  $\alpha_{xy}$  are the irregularity parameters which express the correlation between gradients of the sea surface elevation along spatial and temporal coordinates. Spectral parameters of Eq. 2 describe geometric and kinematic properties of the sea state, for instance the degree of short-crestedness of the sea state  $\gamma_s = L_x/L_y$  (which tends to 0 in long-crested sea states and to 1 in short-crested sea states). Over a given space-time region of volume  $V = XYD$  (with space dimensions  $X$  and  $Y$ , and time duration  $D$ ), the integral parameters are used to define the average number of waves within the volume  $V$  (i.e.,  $N_V$ ), on the surface of the volume  $S$  (i.e.,  $N_S$ ) and over the edge  $P$  (i.e.,  $N_P$ ) (see (Fedele 2012)):

$$N_V = 2\pi \frac{XYD}{L_x L_y T_m} \sqrt{1 - \alpha_{xyt}} \tag{3}$$

$$N_S = \sqrt{2\pi} \left( \frac{XY}{L_x L_y} \sqrt{1 - \alpha_{xy}^2} + \frac{XD}{L_x T_m} \sqrt{1 - \alpha_{xt}^2} + \frac{DY}{T_m L_y} \sqrt{1 - \alpha_{yt}^2} \right) \quad (4)$$

$$N_P = \frac{X}{L_x} + \frac{Y}{L_y} + \frac{D}{T_m} \quad (5)$$

where  $\alpha_{xyt} = \alpha_{xt}^2 + \alpha_{yt}^2 + \alpha_{xy}^2 - 2\alpha_{xt}\alpha_{yt}\alpha_{xy}$ . Following Benetazzo et al. (2015), the probability that the dimensionless maximum second-order sea surface elevation  $Z_2 = \eta_2/\sigma$  ( $\sigma$  being the standard deviation of  $\eta$ ) exceeds a threshold  $z_2$  over a space-time region is obtained as:

$$P(Z_2 > z_2) \approx (N_V z_1^2 + N_S z_1 + N_P) \exp(-z_1^2/2) \quad (6)$$

which, according to Adler and Taylor (2007), holds for large values of  $z_2$ , i.e.  $\eta_2 \gg \sigma$ . Here, the second-order  $z_2$  is a function of the linear elevation  $z_1$  according to the Tayfun (1980) equation

$$z_2 = z_1 + \frac{\mu}{2} z_1^2 \quad (7)$$

where  $\mu$  is an integral measure of the wave steepness. Fedele and Tayfun (2009) provided a statistically stable estimate of  $\mu$  based on the spectral moments:

$$\mu = \mu_o(1 - \nu + \nu^2) = g^{-1} m_{001}^2 m_{000}^{-3/2} (1 - \nu + \nu^2) \quad (8)$$

accounting for the spectral bandwidth  $\nu = \sqrt{m_{000} m_{200} / m_{100}^2} - 1$ , and strictly valid in deep waters ( $g$  being gravitational acceleration). This formulation has been herein adopted also for transitional waters as a first approximation, and preferred to the depth-dependent narrow-band formulation of Tayfun (2006), considering that the effect of water depth on  $\mu$  becomes strong only for very shallow waters.

### 2.1.1 Maximum wave crest height

Assuming that we are dealing with a region in space and time that is large enough to fully capture the dynamics of a wave group, we can reasonably consider  $Z_2$  as the maximum wave crest height in the domain (Fedele 2012). Then, the expected STE crest height  $\bar{Z}_2$  and the standard deviation  $\text{std}(Z_2)$  are obtained according to the asymptotic Gumbel limit of Eq. 6, as shown by Benetazzo et al. (2015) and Fedele (2015):

$$\bar{Z}_2 = \left( \hat{z}_1 + \frac{\mu}{2} \hat{z}_1^2 \right) + \gamma \left[ (1 + \mu \hat{z}_1) \left( \hat{z}_1 - \frac{2N_V \hat{z}_1 + N_S}{N_V \hat{z}_1^2 + N_S \hat{z}_1 + N_P} \right)^{-1} \right] \quad (9)$$

$$\text{std}(Z_2) = \frac{\pi}{\sqrt{6}} \left[ (1 + \mu \hat{z}_1) \left( \hat{z}_1 - \frac{2N_V \hat{z}_1 + N_S}{N_V \hat{z}_1^2 + N_S \hat{z}_1 + N_P} \right)^{-1} \right] \quad (10)$$

where  $\hat{z}_1$  is the largest positive solution of the implicit equation  $(N_V \hat{z}_1^2 + N_S \hat{z}_1 + N_P) \exp(-\hat{z}_1^2/2) = 1$  and  $\gamma \approx 0.5772$

is the Euler Mascheroni constant. According to Gumbel (1958), the 99 % of the realizations of the STE crest height  $Z_2$  should be contained within the interval  $\bar{Z}_2 \pm 3\text{std}(Z_2)$ .

Equations 9 and 10 are an extension of the linear STE model of Fedele (2012) that include the contribution of second-order nonlinearities—see also the nonlinear second-order space extremes model proposed by Fedele et al. (2013). A further extension of the STE model to account for third-order nonlinearities has been recently developed by Fedele (2015), but is not considered in our study because it has not yet been verified against observations; also, it would require the computation of the fourth order cumulants of  $\eta$  and its Hilbert transform: a computationally demanding procedure that, however, does not seem to add significant contributions in most of the cases. Equations 9 and 10 also provide estimates of space or time extreme crests by imposing  $D = 0$ , or  $X = Y = 0$ , respectively.

In the following sections, for practical reasons, we will use the significant wave height  $H_s = 4\sigma$  for normalization (instead of  $\sigma$ ). Hence, the dimensionless expected maximum crest height  $\bar{Z}_2$  will be denoted as  $\bar{\xi}$ , being  $\bar{\xi} = \bar{Z}_2/4$ . Similarly, the standard deviation will be  $\text{std}(\xi) = \text{std}(Z_2)/4$ .

### 2.1.2 Maximum crest-to-trough wave heights

The dimensionless expected STE linear wave height  $\bar{H}_1 = \bar{h}_1/\sigma$  and the wave height associated to the expected STE linear crest height  $\bar{H}_{c,1} = \bar{h}_{c,1}/\sigma$  are estimated according to the QD theory Boccotti (2000), as:

$$\bar{H}_1 = \left[ \hat{z}_1 + \gamma \left( \hat{z}_1 - \frac{2N_V \hat{z}_1 + N_S}{N_V \hat{z}_1^2 + N_S \hat{z}_1 + N_P} \right)^{-1} \right] \sqrt{2(1 - \psi^*)} \quad (11)$$

$$\bar{H}_{c,1} = \left[ \hat{z}_1 + \gamma \left( \hat{z}_1 - \frac{2N_V \hat{z}_1 + N_S}{N_V \hat{z}_1^2 + N_S \hat{z}_1 + N_P} \right)^{-1} \right] (1 - \psi^*) \quad (12)$$

where the term between square brackets in both equations represents the linear estimate of the expected STE crest height, obtained from Eq. 9 with  $\mu = 0$ , and  $\psi^*$  is the first minimum of time autocovariance function of the sea surface elevation  $\psi(\tau)$ .  $\psi^*$  measures the spectral bandwidth, and for wind-generated waves, ranges between  $-0.75$  and  $-0.65$  (Boccotti 2000). The autocovariance function  $\psi(\tau)$  can be computed from the wave spectrum as:

$$\psi(\tau) = \int \int S(\omega, \theta) \cos(\omega\tau) d\omega d\theta = \int S(\omega) \cos(\omega\tau) d\omega \quad (13)$$

where  $\tau$  is time lag,  $S(\omega, \theta)$  is directional spectrum expressed as a function of angular frequency  $\omega$  by means of the transformation  $S(\omega, \theta) = S(k, \theta)/c_g$  ( $c_g$  being the group celerity), and  $S(\omega)$  is the omnidirectional frequency spectrum. The maximum wave height  $H_1$  generally does not correspond to the height of the wave with maximum crest height  $H_{c,1}$ . In stormy wind sea states (typically,  $-0.75 < \psi^* < -0.65$ ), according to Eqs. 11 and 12,  $\bar{H}_1$  is expected to be the 7–10 % larger than  $\bar{H}_{c,1}$ . The ratio decreases as the sea state is more narrow-band. Indeed, for an infinitely narrow-band sea state  $\psi^* = -1$ , hence  $\bar{H}_1 = \bar{H}_{c,1}$ .

The standard deviations of the STE linear wave height, i.e.,  $\text{std}(H_1)$ , and of the wave height associated to the STE linear crest height, i.e.  $\text{std}(H_{c,1})$ , are computed as:

$$\text{std}(H_1) = \left[ \frac{\pi}{\sqrt{6}} \left( \hat{z}_1 - \frac{2N_V \hat{z}_1 + N_S}{N_V \hat{z}_1^2 + N_S \hat{z}_1 + N_P} \right)^{-1} \right] \sqrt{2(1-\psi^*)} \tag{14}$$

$$\text{std}(H_{c,1}) = \left[ \frac{\pi}{\sqrt{6}} \left( \hat{z}_1 - \frac{2N_V \hat{z}_1 + N_S}{N_V \hat{z}_1^2 + N_S \hat{z}_1 + N_P} \right)^{-1} \right] (1-\psi^*) \tag{15}$$

where the term between square brackets in both equations represents the linear estimate of the standard deviation of the STE crest height (obtained from Eq. 10 with  $\mu = 0$ ). Therefore, through Eqs. 14 and 15, the variance of  $H_1$  and  $H_{c,1}$  is related to the intensity function of the linear STE crest probability. The 99th percentile of the realizations of  $H_1$  and  $H_{c,1}$  should be included within the intervals  $\bar{H}_{c,1} \pm 3\text{std}(H_{c,1})$  and  $\bar{H}_1 \pm 3\text{std}(H_1)$ , respectively. Separate space or time extreme wave heights are also obtained from the same equations, by imposing either  $D = 0$ , or  $X = Y = 0$ , respectively.

In the following sections, using  $H_s$  for normalization, the expected maximum linear wave height and the wave height associated to the expected maximum linear crest height will be denoted as  $\bar{\chi} = \bar{H}_1/4$  and  $\bar{\zeta} = \bar{H}_{c,1}/4$ , respectively. Similarly, the standard deviations will be denoted as  $\text{std}(\chi)$  and  $\text{std}(\zeta)$ , respectively.

### 2.2 Observations in the Adriatic Sea

An experiment aimed at observing the occurrence of wave STE was conducted on March 10th, 2014 at the “Acqua Alta” (AA) oceanographic tower (12.5088° E, 45.3138° N, Fig. 1, left panel), in the northern Adriatic Sea (Italy), where a wave acquisition stereo system (WASS, Benetazzo et al. (2012), Fig. 1, right panel) is mounted on the rooftop of the tower, at 12.5 m height. At 09.40UTC, during a well-established north-easterly wind event, known locally as a “Bora” storm, a 30-min-long sequence of stereo images

measured at 15 Hz was recorded over an area of 2893 m<sup>2</sup>. More details of the experiment, equipment set-up, and on the WASS system are provided in Benetazzo et al. (2015).

The WASS stereo system provides a dataset of the sea-surface elevations  $\eta(x, y, t)$  evolving over the two-dimensional space  $(x, y)$ , and time  $(t)$ . As any instrument, WASS has intrinsic sources of error that can affect the overall performance. However, the system is well-known for its high accuracy, with 3 cm maximum error along each axis in the AA tower configuration. Prior to analysis, the stereo dataset is typically treated in order to limit the effects of high-frequency noise on the observed  $\eta$  and on derived quantities (e.g., the directional spectrum). Therefore, time series of sea surface elevation  $\eta(x_0, y_0, t)$  taken at each position  $(x_0, y_0)$  of the 3D stereo dataset were smoothed using a weighted linear least squares local regression and low-pass filtered at 2.0 Hz. The resulting  $\eta$  were employed for STE detection and for directional spectrum estimation (see Fig. 5) using the extended maximum entropy principle (EMEP, Hashimoto et al. (1994)), in a way that synthetic characteristics of the sea state could be assessed (Table 1).

The observed storm event generated a fetch-limited sea state with significant wave height  $H_s = 1.33$  m, mean wave propagation direction  $\theta_m = 248^\circ$  N, and peak period  $T_p = 5.2$  s. The sea state was short-crested, as indicated by  $\gamma_s = 0.93$ , and it was quite random along the wave propagation direction, as pointed out by the rather small value of  $\alpha_{xt}$ , thus implying likelihood of encountering large waves (compared to  $H_s$ ). Steepness  $\mu = 0.06$  and first minimum of the autocovariance function  $\psi^* = -0.67$  are typical values during wind-generated sea states. The first indicates that second-order nonlinearities played a significant role in the statistics of extreme crests, the second points out that the sea state was not narrow-band in frequency. Therefore, the profile of the highest waves was expected to be markedly asymmetric, and the maximum wave height was expected to be 9 % larger than the wave height associated to the maximum crest.

During the experiment, 23 waves with crest height exceeding the freak wave threshold (i.e.,  $\xi > 1.25$ , Dysthe et al. (2008)) were observed over the area. The empirical excee-

**Table 1** Observed (WASS) wave parameters at AA tower on March 10th, 2014, 09.40UTC–10.10UTC

$H_s$ (m)	$\theta_m$ (°N)	$\theta_p$ (°N)	$T_m$ (s)	$T_p$ (s)
1.33	248	254	3.6	5.2
$L_x$ (m)	$L_y$ (m)	$\alpha_{xt}$	$\alpha_{yt}$	$\alpha_{xy}$
13.6	14.6	0.35	0.04	0.03
$\nu$	$\mu$	$\psi^*$	$\sigma_s$ (°)	$\gamma_s$
0.47	0.06	-0.67	23	0.93

dence distribution of  $\xi$ , based on the integral spectral parameters, was found to be fairly represented by the right tail of the distribution of Eq. 6 (i.e., for large thresholds), on a volume  $V_1$  of duration  $D = 1800$  s and area  $XY = 11.2 \cdot 11.2 = 126 \text{ m}^2$ , which is the area pertaining on average to each of the 23 waves homogeneously distributed within the total observed area (see Figure 9 of Benetazzo et al. (2015)). The observed STE crests (dimensionless, Table 2) ranged between 1.25 and 1.59, with a mean value  $\bar{\xi} = 1.38$  (i.e., significantly over the freak wave threshold) and standard deviation  $\text{std}(\xi) = 0.09$ . The 23 associated crest-to-trough heights (dimensionless, Table 2) ranged between 1.79 and 2.42, with a mean value  $\bar{\zeta} = 2.08$  and standard deviation  $\text{std}(\zeta) = 0.16$ . Theoretical expectations from Eqs. 9 and 12 were 1.37 and 2.01, respectively; thus, in fair agreement with mean values of observations (Table 2), being only 1 and 3 % lower, respectively.

In the same experiment, STE crest and corresponding wave height were also observed on a different space-time volume  $V_2$  obtained by dividing the observed field of view in four subareas ( $XY = 30.6 \cdot 30.6 = 936.4 \text{ m}^2$ ) and the duration in four subintervals ( $D = 450$  s). The STE crests (dimensionless, Table 2), whose exceedance distribution was in fair agreement with the right tail of Eq. 6, varied between 1.06 and 1.64, with a mean value  $\bar{\xi} = 1.38$  (coincidentally equal to the value for  $V_1$ ) and standard deviation  $\text{std}(\xi) = 0.17$ ; while corresponding wave height (dimensionless, Table 2) ranged between 1.44 and 2.51, with a mean value  $\bar{\zeta} = 2.02$  and standard deviation  $\text{std}(\zeta) = 0.28$ . Again, theoretical expectations agreed well with mean values of observations:  $\bar{\xi} = 1.42$  (i.e., 3 % higher) and  $\bar{\zeta} = 2.06$  (i.e., 2 % higher).

### 3 Space-time extremes implementation in WAVEWATCH III

The WAVEWATCH III® (WW3) wind wave model solves the random-phase spectral action density balance equation for wavenumber-direction spectra (Tolman 1991). Several source-term packages allow computing wave generation by wind, decay by dissipative processes, nonlinear wave-wave

**Table 2** Observed (WASS) dimensionless STE at AA tower on March 10th, 2014, 09.40UTC–10.10UTC, over regions  $V_1$  ( $X = Y = 11.2$  m,  $D = 1800$  s) and  $V_2$  ( $X = Y = 30.6$  m,  $D = 450$  s): maximum crest height  $\xi$  and height of the wave with maximum crest height  $\zeta$

	$\xi$				$\zeta$			
	Min	Mean	Max	std	Min	Mean	Max	std
$V_1$	1.25	1.38	1.59	0.09	1.79	2.08	2.42	0.16
$V_2$	1.06	1.38	1.64	0.17	1.44	2.02	2.51	0.28

interactions, and wave transformation near the coast. The STE computation has been integrated to WW3 in modules and subroutines dealing with model output and post-processing. Modifications have been also made to properly initialize STE output fields, and ensure data integrity when using parallel processing environments. The STE implementation herein presented is distributed with the WW3 version 5.16 (WW3DG 2016), which is made available to the general public through the WW3 website.<sup>1</sup>

The procedure implemented in WW3 follows the path described in Section 2. First, the directional spectrum computed by the model is integrated in order to get the spectral moments of Eq. 1. Only the prognostic part of the spectrum is considered, without adding any diagnostic spectral tail. As we want integral parameters with respect to the mean wave direction of propagation  $\theta_m$  (e.g., to estimate the short-crestedness  $\gamma_s$ ), we consider a rotated ( $\hat{x}, \hat{y}$ ) reference frame where direction  $\theta$  is turned to  $\hat{\theta} = \theta - \theta_m$ . Thus, wavenumber components ( $k_x, k_y$ ) become

$$\begin{aligned} k_{\hat{x}} &= k \cos \hat{\theta} = k \cos(\theta - \theta_m) \\ &= k(\cos \theta \cos \theta_m + \sin \theta \sin \theta_m) \\ k_{\hat{y}} &= k \sin \hat{\theta} = k \sin(\theta - \theta_m) \\ &= k(\sin \theta \cos \theta_m - \cos \theta \sin \theta_m) \end{aligned}$$

having applied trigonometric identities. Therefore, the integral parameters follow from Eq. 2 and the wave steepness  $\mu$  from Eq. 8. Although integral parameters are different in the original model and rotated reference frames, expected STE are not affected by the rotation (Benetazzo et al., 2016, Space-time extreme wind waves: analysis and prediction of shape and height, unpublished).

Next, integral parameters are used together with user-defined space-time region size (namely,  $X, Y, D$ ) to compute the average numbers of 3D, 2D, and 1D waves, i.e., Eqs. 3–5. If not specified, default values of region size are used,  $X = Y = 1000$  m,  $D = 1200$  s.

The expected STE crest  $\bar{Z}_2$  and the standard deviation  $\text{std}(Z_2)$  are computed from Eqs. 9 and 10, respectively, after the mode of the probability distribution  $\hat{z}_1$  is estimated as:

$$\hat{z}_1 \approx \sqrt{2 \ln(N_V) + 2 \ln(2 \ln(N_V) + 2 \ln(2 \ln(N_V)))} \quad (16)$$

This expression, derived in accordance with Krogstad et al. (2004) and Socquet-Juglard et al. (2005), approximates the largest positive solution of  $(N_V z_1^2 + N_S z_1 + N_P) \exp(-z_1^2/2) = 1$ . It strictly holds on large areas, i.e., if  $XY \gg L_x L_y$ , but can be considered a good approximation also on smaller areas. Indeed, assuming for instance a JONSWAP spectrum (Hasselmann et al. 1973) and  $\cos^2$  directional distribution, the error with respect to the mode

<sup>1</sup><http://polar.ncep.noaa.gov/waves/wavewatch.shtml>

obtained as the exact solution of the implicit equation is 1 % for  $X/L_x = 1$  and fall below 0.1 % for  $X/L_x > 15$ . In case space-only ( $D = 0$ ) or time-only ( $X = Y = 0$ ) extremes are desired, the model is approximated as either  $\hat{z}_1 \approx \sqrt{2 \ln(N_S) + \ln(2 \ln(N_S) + \ln(2 \ln(N_S)))}$ , or  $\hat{z}_1 \approx \sqrt{2 \ln(N_P)}$ , respectively.

The expected STE wave heights  $\bar{H}_1$  and  $\bar{H}_{c,1}$ , and standard deviations  $\text{std}(H_1)$  and  $\text{std}(H_{c,1})$  are computed from Eqs. 9, 10 and 14, 15 after the first minimum of the autocovariance function  $\psi^*$  is estimated. In order to reduce the computational effort and keep runtime as low as possible, autocovariance function is obtained using an ad-hoc algorithm that computes Eq. 13. First, only the portion of the time-lag axis  $\tau$  where it is more likely to encounter the minimum is retained. Hence, the model computes 21 values of  $\psi(\tau)$  for  $0.3T_m \leq \tau \leq T_m$ . Indeed, according to Boccotti (2000), the period of the highest waves in a JONSWAP-like sea state (peak-enhancement factor 3.3) is approximately  $0.92T_p \approx 1.3T_m$  (taking  $T_p \approx 1.41T_m$ ) and so the minimum is typically expected at  $\tau \approx 0.65T_m$ , since the crest of the wave occurs at  $\tau = 0$ . Also, the number of iterations to integrate the frequency spectrum  $S(\omega)$  has been reduced to one fourth by virtue of the following integration algorithm:

```
for j = 1,21, step 1 do
  for i = 1, nω, step 4 do
```

$$\begin{aligned} \psi(\tau_j) = & \psi(\tau_j) + \delta^3 S(\omega_{i+3}) \cos(\delta^3 \omega_i \tau_j) \\ & + \delta^2 S(\omega_{i+2}) \cos(\delta^2 \omega_i \tau_j) \\ & + \delta S(\omega_{i+1}) \cos(\delta \omega_i \tau_j) \\ & + S(\omega_i) \cos(\omega_i \tau_j) \end{aligned}$$

```
  end for
end for
```

that while adding the contribution of the  $i$ th frequency to the integral, at the same time retains the contribution of the  $(i + 1)$ th,  $(i + 2)$ th, and  $(i + 3)$ th frequencies. Herein,  $n\omega$  is the number of wavenumbers/frequencies adopted, and  $\delta$  is the ratio between subsequent frequencies (e.g., 1.1). The reduction factor 4 has been chosen as, typically, 32, 36, or 40 frequencies are used to represent the spectral space in wave models.

In the WW3 implementation, STE parameters are provided as dimensional variables by means of  $\sigma = \sqrt{m000}$ . The new output parameters, namely the expected STE and standard deviations, are STMAXE (i.e.,  $\bar{\eta}_2$ ), STMAXD (i.e.,  $\text{std}(\eta_2)$ ), HMAXE (i.e.,  $\bar{h}_1$ ), HMAXD (i.e.,  $\text{std}(h_1)$ ), HCMAXE (i.e.,  $\bar{h}_{c,1}$ ), and HCMAXD (i.e.,  $\text{std}(h_{c,1})$ ). A first validation of STE parameters computed within the WW3 model, relative to the AA tower STE measurements, is provided next.

## 4 Test case: “Acqua Alta” wave extremes

### 4.1 Model setup

In order to simulate with WW3 the wave conditions during the AA experiment, a curvilinear Lambert conformal grid was set-up on the Mediterranean Sea with 5-km resolution. The bathymetric domain was obtained by interpolating the EMODNET bathymetry dataset (1/8° x 1/8°, www.emodnet-bathymetry.eu) on the grid (Fig. 2). Directional wave spectra were discretized using a constant 10° directional increment (covering all directions), and a spatially varying wavenumber grid (corresponding to an invariant logarithmic intrinsic frequency grid covering from 0.05 to 2.00 Hz, i.e., deep water wave components in the 0.5 to 20.0 s range, the same range used in the WASS experiment). The source-term package of Ardhuin et al. (2010) was used for wave growth and decay, in association with the discrete interactions approximations (DIA) of Hasselmann et al. (1985) for nonlinear wave-wave interactions. Propagation was computed using a third-order accurate scheme. Subgrid-scale obstructions, such as islands and coastal features, were included. Near the coast, bottom friction was modeled using the JONSWAP parameterization (Hasselmann et al. 1973), as well as the depth-induced wave breaking parameterization of Battjes and Janssen (1978).

According to Signell et al. (2005), the high resolution of atmospheric models (e.g., horizontal grid size smaller than 20 km) is crucial to improve the accuracy of numerical wave model forcings in semi-enclosed basins as the Adriatic Sea, as it adequately addresses the effect of the surrounding orography on dominant and transient winds. Therefore, WW3 was forced by horizontal wind-field components at 10-m height produced by the “Consortium for small Scale MOdeling-MEDiterranean” (COSMO-ME, Steppeler et al. (2003)) atmospheric model, an operational version of the non-hydrostatic regional COSMO model, run by CNMCA within the NETTUNO forecasting system (Bertotti et al. 2013). COSMO-ME is integrated over the European-Mediterranean area with 7-km horizontal grid resolution and 40 vertical levels, using the LETKF-CNMCA data assimilation system fields as initial conditions and the IFS fields as lateral boundary conditions. Forecasting fields are produced twice a day (00 UTC and 12 UTC) over 72 h, with 3-h resolution. For our study, we used the COSMO-ME wind fields covering the March 02–30, 2014 period.

The sea state observed by WASS at “Acqua Alta” is part of a northeasterly “Bora” storm lasting approximately 1.5 day, from March 10th, 2014 at 00.00UTC to March 11th, 2014 at 12.00UTC (see, e.g., Fig. 3), a typical duration of storms driven by Bora winds in the Adriatic Sea. However, in order to assess the model performance, WW3 was run for the whole March 02–30, 2014 period (neglecting the first 48-h warm-up), producing hourly output wave parameters.

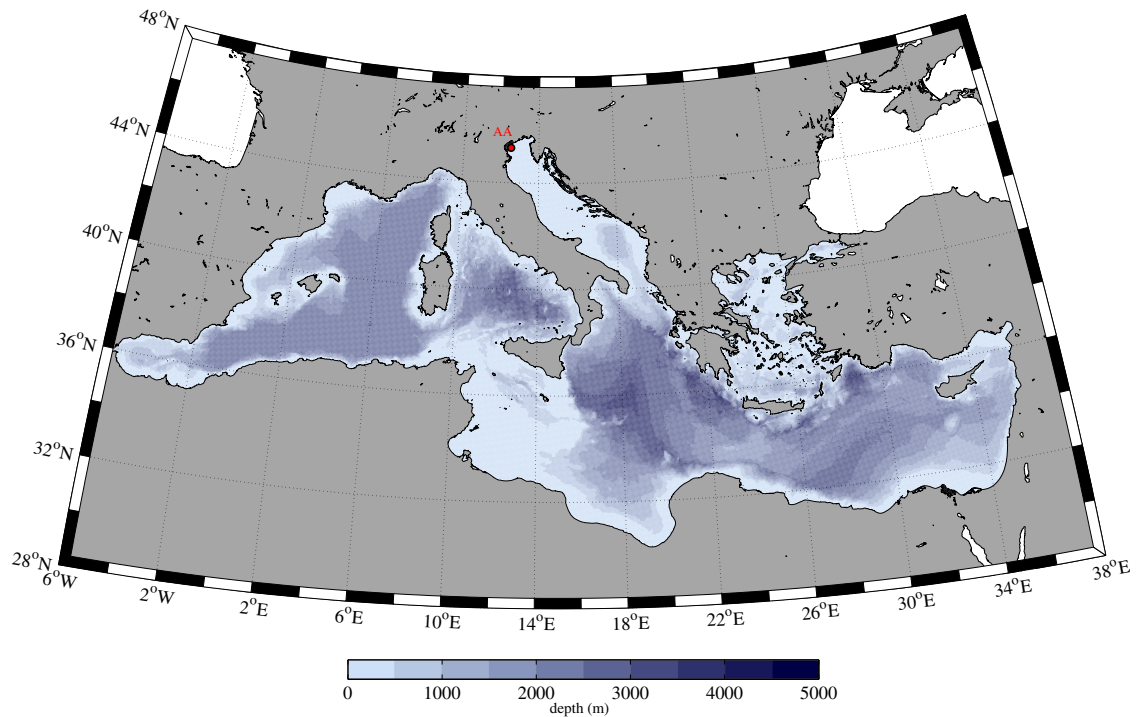


**Fig. 2** WW3 computational domain and interpolated bathymetry of the Mediterranean Sea. AA (red) is “Acqua Alta” tower location, in the northern Adriatic Sea

## 4.2 Model-observation comparisons

Surface winds from the COSMO-ME model, and wave results from the WW3 model were compared to data gathered at the AA tower. We focused on this station because the storm under analysis was localized in the Adriatic Sea, mostly in the northern part of the basin. Atmospheric AA data are provided by a T031-TVV/T033-TDV SIAP anemometer (measuring wind speed and direction every 5 min at 15-m height, with 0.5 m/s and 0.5° accuracy). Wind speed is then corrected to the standard 10-m reference level, assuming near-neutral conditions, and wind directions rotated in order to align to the wave convention (i.e., directions of propagation, with respect to geographical North). Wave data are routinely measured at AA by an acoustic surface tracking system (Nortek Acoustic

Wave and Current profiler, AWAC) at 1-Hz sampling frequency and with an accuracy of 1 % of the measured value for wave elevation and 2° for wave direction.

The comparison of modeled and observed atmospheric parameters is provided in Fig. 3 and in Table 3. For assessment, we used the correlation coefficient (CC), root mean square error (RMSE) and model-observation Bias for wind speed  $U_{10}$ , and directional model-observation bias (Bias°) for wind direction  $\theta_U$  (according to Mardia and Jupp (2009)). As verified by Bertotti et al. (2013), performance of COSMO-ME at the tower is quite good, despite the intrinsic error typically accompanying forecasts. Indeed, the wind is globally well reproduced with  $U_{10}$  having CC of 0.86, RMSE of 1.81 m s<sup>-1</sup>, and Bias of -0.01 m s<sup>-1</sup>. Wind direction  $\theta_U$  is slightly positively biased (1.39°).

**Fig. 3** COSMO-ME atmospheric outputs (inputs for WW3, black) and observations (gray) at AA tower: wind speed (left) and direction (right) at 10-m height. The red lines denote the WASS stereo experiment. Wind directions denote where the wind is blowing to (in agreement with the wave direction convention)

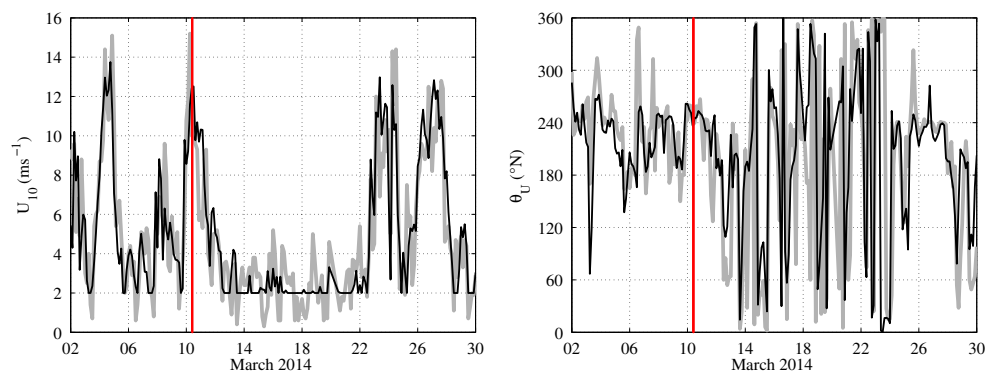




**Table 3** Comparison of atmospheric and wave parameters at AA tower, as statistical indicators of the agreement between modeled and observed parameters: correlation coefficient (CC), root mean square error (RMSE) and model-observation Bias for wind speed  $U_{10}$ , significant wave height  $H_s$ , mean wave period  $T_m$ ; directional model-observation Bias $^\circ$  for wind direction  $\theta_U$  and mean wave direction  $\theta_m$  (according to (Mardia and Jupp 2009)). Compared period is March 02–30, 2014 for COSMO-ME, and March 04-30, 2014 for WW3

		CC	RMSE	Bias	Bias $^\circ$ ( $^\circ$ )
COSMO-ME	$U_{10}$ ( $\text{m s}^{-1}$ )	0.86	1.81	-0.01	-
	$\theta_U$ ( $^\circ$ N)	-	-	-	1.39
WW3	$H_s$ (m)	0.92	0.19	-0.06	-
	$T_m$ (s)	0.76	0.59	-0.40	-
	$\theta_m$ ( $^\circ$ N)	-	-	-	5.54

With respect to observations, the storm under investigation is simulated with smaller wind speed at the peak ( $12.5 \text{ m s}^{-1}$  instead of  $15.2 \text{ m s}^{-1}$ ), which verifies 6 h later than the actual occurrence. This is not surprising, as on the one hand it is recognized that atmospheric models systematically underestimate short-fetch winds (as Bora) in enclosed basins (as the northern Adriatic Sea, see Cavaleri and Bertotti (2004)); on the other, COSMO-ME is a forecasting model, whose performance on the whole Adriatic Sea was assessed by Bertotti et al. (2013) finding CC of 0.85, RMSE of  $1.80 \text{ m s}^{-1}$  and Bias of  $-0.29 \text{ m s}^{-1}$  (values that very well resemble the statistics we obtained at AA over a shorter period, but with a higher Bias). Wind direction

$\theta_U$  at the peak is simulated with a  $14^\circ$  difference with respect to observations ( $245^\circ$  N instead of  $259^\circ$  N). However, during the WASS experiment, observed and modeled  $U_{10}$  are  $10.7$  and  $12.2 \text{ m s}^{-1}$ , respectively, while  $\theta_U$  is accurately reproduced ( $239^\circ$  N).

The comparison of modeled and observed wave parameters is provided in Fig. 4 and in Table 3. For assessment, we used CC, RMSE, and model-observation Bias for significant wave height  $H_s$  and mean wave period  $T_m$ , and model-observation Bias $^\circ$  for mean wave direction  $\theta_m$ .  $H_s$  is reproduced with CC of 0.92, RMSE of 0.19 m and Bias of  $-0.06 \text{ m}$ .  $T_m$  has CC of 0.76, RMSE of 0.59 s and Bias of  $-0.40 \text{ s}$ . Hence, as a consequence of the wind underestimate (at AA and most likely over the whole Bora fetch), simulated  $H_s$  and  $T_m$  are generally smaller than the observations, in particular  $T_m$ .  $\theta_m$  is slightly rotated, having a Bias $^\circ$  of  $5.54^\circ$ . With respect to observations, the storm is reproduced with smaller  $H_s$  (1.68 m, instead of 1.97 m) and  $T_m$  (4.0 s, instead of 4.2 s) at the peak, retaining the 6 h delay already observed in  $U_{10}$ . Modeled  $\theta_m$  at the peak ( $253^\circ$  N) is  $6^\circ$  far from the observation ( $259^\circ$  N). During the WASS experiment, the modeled storm is still in its growing phase (in contrast with observations) and has  $H_s = 1.60 \text{ m}$ ,  $T_m = 3.9 \text{ s}$  and  $\theta_m = 261^\circ$  N (Table 4), while  $H_s = 1.33 \text{ m}$ ,  $T_m = 3.6 \text{ s}$  and  $\theta_m = 248^\circ$  N have been observed with WASS in the storm descent.

Hence, we can conclude that the atmospheric and wave parameters at AA are generally well reproduced by the

**Fig. 4** WW3 wave outputs (black) and observations (gray) at AA tower: significant wave height (top-left), mean wave period (top-right) and mean wave direction (bottom). The red lines denote the WASS stereo experiment

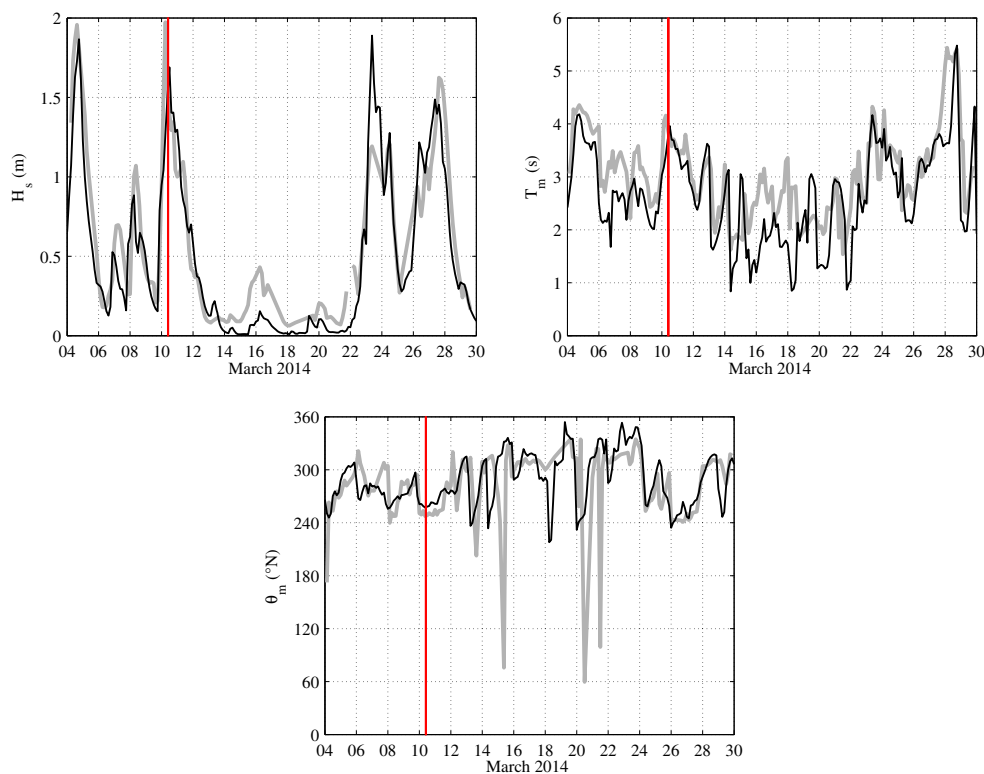


**Table 4** Modeled (WW3) wave parameters at AA tower on March 10th, 2014, 10.00UTC

$H_s$ (m)	$\theta_m$ (°N)	$\theta_p$ (°N)	$T_m$ (s)	$T_p$ (s)
1.60	261	265	3.9	5.8
$L_x$ (m)	$L_y$ (m)	$\alpha_{xt}$	$\alpha_{yt}$	$\alpha_{xy}$
17.0	20.6	0.80	-0.14	-0.13
$\nu$	$\mu$	$\psi^*$	$\sigma_s$ (°)	$\gamma_s$
0.45	0.07	-0.64	27	0.83

COSMO-ME and WW3 modeling system. However, during the Bora storm, some discrepancies have been found, in particular at the peak and during the experiment. Such discrepancies, partly resulting from deficiencies in the wind forcing, suggest differences between modeled and observed directional spectra that will be discussed later on in Section 4.3, as they in turn reflect in differences on STE results from the model.

### 4.3 Results

The STE results of the WW3 model are analyzed in this section. We consider WW3 outputs at 10.00 UTC on March 10th, 2014 for comparison with WASS observations of maxima at AA (between 09.40 UTC and 10.10 UTC). First, we describe and compare results in terms of directional spectra and spectral parameters, which are used by WW3 for STE estimate. Taking into account the directional spectra, we assume there is no effect of the spectral resolution, as shown by Benetazzo et al. (2016, Space-time extreme wind waves: analysis and prediction of shape and height, unpublished) who found, for instance, an excellent agreement between the autocovariance function  $\psi(\tau)$  computed from the original WASS spectrum (1024 frequencies and 180 directions) and that computed from the WASS spectrum with a model-type resolution (i.e., 40 frequencies and 36 directions). Then, we present STE model results, and discuss them in the light of the spectral and parameter difference found, whilst comparing them with observations.

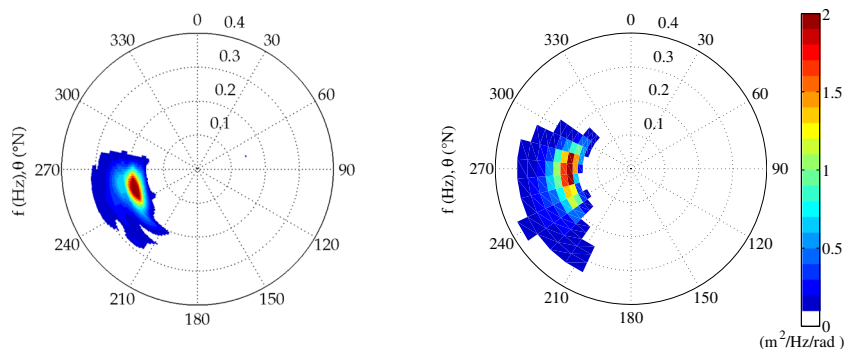
#### 4.3.1 Wave spectra and parameters

The directional spectrum at AA computed by WW3 at 10.00 UTC is depicted in Fig. 5, where, for comparison, the WASS spectrum is also shown. Directional spectra (modeled and observed) have been computed in the same frequency range (0.05–2.00 Hz, and 0–360° N). Integral and peak parameters of the modeled spectrum are collected in Table 4 and have to be compared with observed parameters in Table 1. As seen, both spectra are unimodal, with comparable spectral levels at the peak. However, the modeled spectrum is wider both in frequency and direction with respect to the observed spectrum. This is consistent with the larger  $H_s$  and  $T_m$  computed by the model (due to the different wind). For the same reason, also the model mean wavelength  $L_x$  and mean wave crest  $L_y$  are larger than those from observations: 17.0 m in place of 13.6 m for  $L_x$ , and 20.6 m in place of 14.6 m for  $L_y$ . This leads to a less short-crested sea state: indeed  $\gamma_s$  is 0.83, while we computed 0.93 during observations.

Peak period is 5.8 s (WW3) instead of 5.2 s (WASS). The modeled spectrum is also slightly rotated toward west with respect to the observed one ( $\theta_p = 265^\circ$  N instead of  $254^\circ$  N, and  $\theta_m = 261^\circ$  N instead of  $248^\circ$  N), as a consequence of a positively biased wind direction during the simulation. Irregularity parameters show some differences: indeed  $\alpha_{xt}$ , which expresses the correlation between the space and time gradients of the sea surface elevation in the wave propagation direction, is much larger in model results (0.80 instead of 0.35). This means that the modeled sea state should be more organized along the propagation direction with respect to observations. Also  $\alpha_{yt}$  and  $\alpha_{xy}$  parameters are larger in model results and they are negative. However, despite these differences, their absolute values remain smaller than  $\alpha_{xt}$ .

In order to compare the spectral shapes computed by the model and those obtained from stereo observations, we derive the omnidirectional frequency spectra  $S(f)$  and the directional distribution functions  $D(\theta)$ , which are shown in Fig. 6. For a better comparison of  $S(f)$  and  $D(\theta)$ , the model spectrum is also scaled with the observed variance (i.e., the observed  $S(f)$  integral) and shifted of 0.02 Hz

**Fig. 5** Observed (left,  $\Delta f = 2 \cdot 10^{-3}$  Hz,  $\Delta \theta = 2^\circ$ ) and modeled (right,  $\Delta f/f = 0.1$ ,  $\Delta \theta = 10^\circ$ ) directional wave spectrum  $S(f, \theta)$  during the WASS experiment, in the 0.05–2.00 Hz and 0–360° ranges. In Figure, only the 0.05–0.40 Hz range is shown for clarity



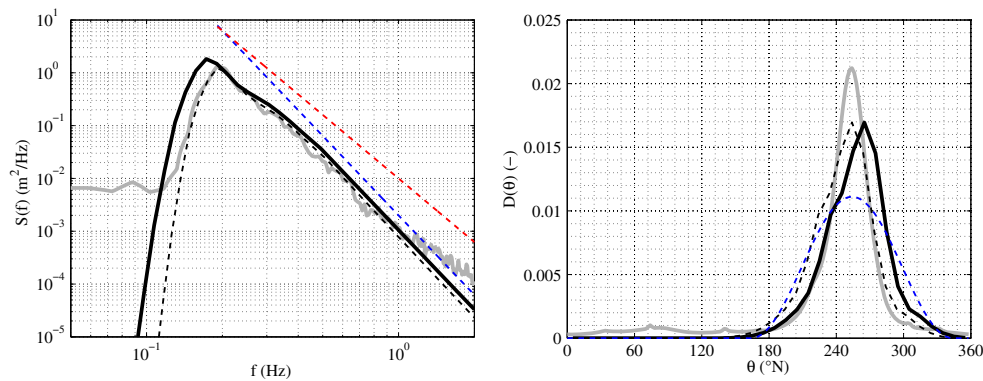


**Fig. 6** Omnidirectional frequency spectrum  $S(f)$  (left) and directional distribution function  $D(\theta)$  (right): observed (gray solid line) and modeled (black solid line). For comparison, modeled spectrum is scaled and shifted (0.02 Hz) to match the observed total variance and peak frequency (black dashed line), and modeled directional

distribution is shifted ( $11^\circ$ ) to match the observed peak direction (black dashed line). Reference spectral slopes are shown as red dashed line ( $f^{-4}$ ) and blue dashed line ( $f^{-5}$ ) in the left panel. Reference directional distribution ( $D(\theta) = \Gamma \cos^{2s}(\theta)$ , with  $s = 1$  and  $\Gamma$  the normalization factor) is shown as blue dashed line in the right panel

to have comparable spectral levels and aligned peaks, and the model distribution is also rotated of  $11^\circ$  to align the peaks. The shapes of modeled and observed  $S(f)$  are almost corresponding in the range 0.15–1.00 Hz. Above this range, a residual noise is visible in the observation spectrum causing it to depart from the slope it follows until there, in agreement with reference spectral slopes.

Hence, overall, the spectral width reproduced by the model is very similar to the observed one, though slightly larger, as also indicated by  $\nu$  (0.45 instead of 0.47) and  $\psi^*$  ( $-0.64$  instead of  $-0.67$ ). The integral steepness  $\mu$  is well reproduced, being 0.07 from the model spectrum and 0.06 from the observed spectrum. The directional distribution simulated by WW3 is wider than that observed. Also, while the latter is almost symmetric about the peak, model distribution exhibits a larger extension toward the southern directions ( $180^\circ$  N). These features are synthesized by the directional spreading parameter  $\sigma_s$  (Kuik et al. 1988), that is equal to  $23^\circ$  for observations (retaining the  $\theta_p \pm 90^\circ$  range only, to limit the noise introduced by EMEP) and to  $27^\circ$  for model distribution (the  $\cos^{2s}$  distribution with  $s = 1$  and  $\sigma_s = 31^\circ$  is also plotted in Fig. 6 for reference).

### 4.3.2 Space-time wave extremes

Given the modeled directional spectrum and the integral parameters associated, we expect the modeled STE to be smaller than the observed ones. Indeed, it is evident from Eqs. 3–5 that for the same space-time volume (i.e.,  $V_1$  or  $V_2$ ) by virtue of larger  $L_x$ ,  $L_y$ ,  $T_m$ ,  $\alpha_{xt}$ ,  $\alpha_{yt}$ , and  $\alpha_{xy}$ , the average numbers of waves (i.e.,  $N_V$ ,  $N_S$ ,  $N_P$ ) are smaller. In turn, Eq. 9 gives smaller expected STE crests. For the same reason, and also due to the smaller modeled  $\psi^*$ , the computed expected STE wave height from Eq. 11 and the wave

height associated to the expected STE crest from Eq. 12 are smaller too.

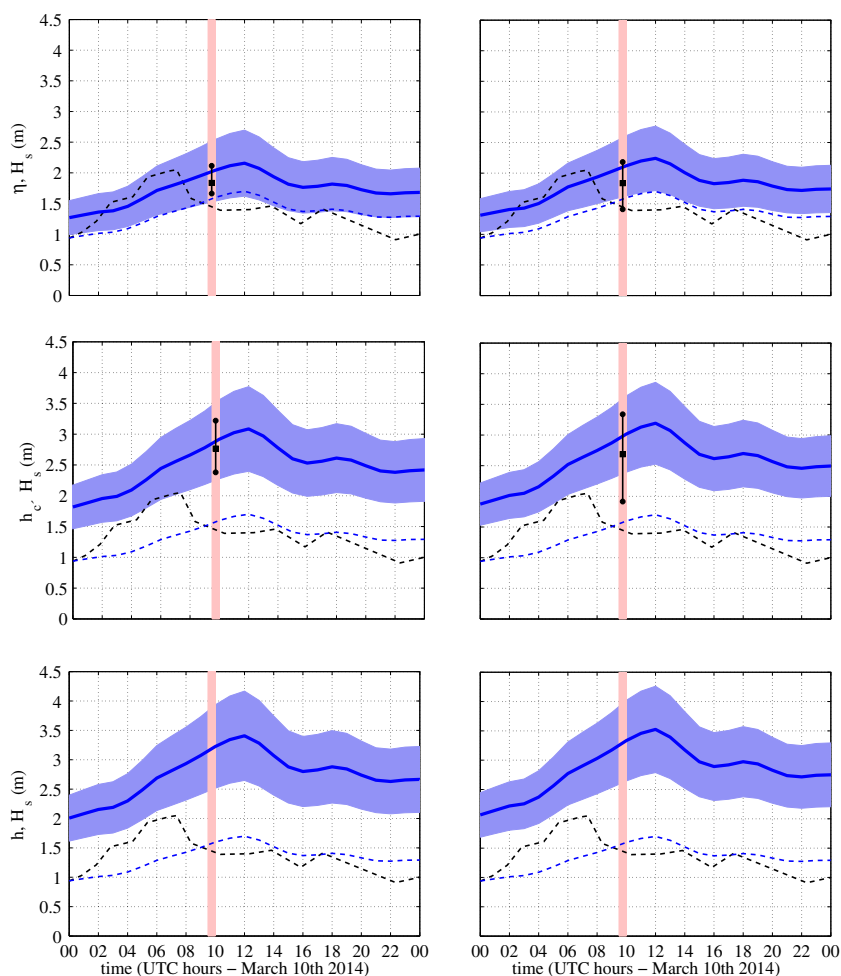
STE computed by the WW3 model are collected in Table 5 (to be compared with observed STE in Table 2). Over  $V_1$ , WW3 computed a  $\bar{\xi}$  of 1.28 and a  $\bar{\zeta}$  of 1.83, whereas STE from WASS were  $\bar{\xi} = 1.38$  and  $\bar{\zeta} = 2.08$ . Hence, WW3 underestimated the STE of 7 and 12 %, respectively. Over  $V_2$ , modeled  $\bar{\xi}$  is 1.33 and  $\bar{\zeta}$  is 1.89, while observed  $\bar{\xi}$  is 1.38 and  $\bar{\zeta}$  is 2.02. Thus, WW3 underestimated the STE of 4 and 6 %, respectively. The expected maximum wave heights  $\bar{\chi}$  over  $V_1$  and  $V_2$  (not compared to observations) were 2.02 and 2.09, respectively. Hence, as expected, given  $\psi^* = -0.64$ , modeled  $\bar{H}_{c,1}$  is 9 % smaller than  $\bar{H}_1$ , for both the space-time regions.

In Fig. 7, the time-series of the dimensional STE computed by WW3 on March 10th, 2014 are plotted. As seen, the time evolution of the expected STE are strongly correlated with the time evolution of  $H_s$ . Also, the confidence intervals (i.e.,  $\pm 3$ std with respect to expected values) widen in correspondence of large  $H_s$  values, e.g., at the storm peak, and tighten where  $H_s$  is lower. Observed STE are depicted as mean values and bars extending from the minimum to

**Table 5** Modeled (WW3) dimensionless STE at AA tower on March 10th 2014, 10.00UTC, over regions  $V_1$  ( $X = Y = 11.2$  m,  $D = 1800$  s) and  $V_2$  ( $X = Y = 30.6$  m,  $D = 450$  s): maximum crest height  $\xi$ , height of the wave with maximum crest height  $\zeta$  and maximum wave height  $\chi$

	$\xi$		$\zeta$		$\chi$	
	Mean	std	Mean	std	Mean	std
$V_1$	1.28	0.11	1.83	0.13	2.02	0.15
$V_2$	1.33	0.10	1.89	0.13	2.09	0.14

**Fig. 7** Time series of modeled dimensional STE at AA on March 10th, 2014, over the regions  $V_1$  ( $X = Y = 11.2$  m,  $D = 1800$  s, *left panels*) and  $V_2$  ( $X = Y = 30.6$  m,  $D = 450$  s, *right panels*): maximum crest height ( $\eta$ , *top panels*), height of the wave with maximum crest height ( $h_c$ , *central panels*) and maximum wave height ( $h$ , *bottom panels*), depicted as expected values (*blue solid line*) and confidence intervals ( $\pm 3$ std, *blue filled area*). Observations are drawn as mean (*black square*), minimum and maximum values (*black circles*). Observed (*black dashed line*) and modeled (*blue dashed line*) significant wave heights are also drawn in each panel. The WASS stereo experiment duration is highlighted by the *light red bar*



the maximum observed values. For  $V_1$ , observations are included within the model confidence interval; for  $V_2$  the mean and maximum values stay within the interval, while minimum observed crest and associated wave height fall outside of the confidence interval. As shown, the model  $H_s$  differs from the observed one, especially in the first 8 h of the day, when observations reach the peak while modeled storm is still growing. During the experiment, differences reduce and modeled  $H_s$  is higher than observed (1.60 m instead of 1.33 m). However, due to such differences and higher modeled  $H_s$ , model dimensional STE are higher than the observed ones. Precisely, over  $V_1$  the expected STE crest and associated wave height are overestimated of 11 and 6 %, respectively; over  $V_2$  of 16 and 12 %, respectively.

## 5 Discussion and conclusions

In this study, we have presented the implementation of a STE model for ocean wind waves within WW3 version 5.16, and validated simulation results with stereo observations of open-ocean waves as first test case for the

novel implementation. For the present purpose, we have introduced in WW3 the STE model of Fedele (2012) as extended by Benetazzo et al. (2015) to predict the second-order nonlinear crest height, and the linear QD theory of Boccotti (2000) to predict the STE wave heights. Sea-state parameters and extremes during a storm in the Mediterranean Sea have been simulated by WW3 forced by wind fields provided by the COSMO-ME atmospheric model. Observations of sea-state extremes have been gathered in the northern Adriatic Sea (Italy), at the oceanographic tower “Acqua Alta,” by a stereo system WASS, providing STE over two different space-time regions.

Results of the test case have shown that the WW3 STE model predictions are in agreement with the real-case WASS observation, being dimensionless STE crest and wave heights as accurate as (at most) 7 and 12 %, respectively. Observed model-observation discrepancies are due to the combination of errors of different sources, namely forcing wind fields, WW3 model source term parameterizations, the STE theoretical model, and the STE implementation. During the WASS experiment, the STE theoretical model herein considered was shown to be accurate to within the

3 % (at most) of the observed STE crest and associated wave heights. In the following, we focus our discussions on the conditions in which results have been obtained and on the effects of the model approximations and model forcing.

Model-observation discrepancies are mainly related to the effect of the wind forcing on the directional spectrum. Indeed, despite a general agreement with observations at AA over the simulation, the peak of the storm in study (both in terms of  $U_{10}$  and of spectral wave parameters, which directly depends on  $U_{10}$  as the storm was dominated by wind seas without swells from other regions) is postponed and underestimated. The larger modeled wind speed during the experiment causes the computed parameters ( $H_s$ ,  $L_x$ ,  $L_y$ ,  $T_m$ ,  $\alpha_{xt}$ ,  $\alpha_{yt}$ , and  $\alpha_{xy}$ ) to be different and, in particular, larger than those observed. For instance, modeled  $H_s$  is 20 % larger than the observed one. To show that a better representation of the directional spectrum (and so, of wave parameters) would lead to better agreement with observations, in Table 6 we combine the STE estimate implemented in WW3 with the best spectrum we can get from the model, i.e., the WASS directional spectrum interpolated on the model spectral grid. From the comparison with Table 5, we see that the observed-modeled discrepancy in expected STE crest heights  $\xi$  reduces from 7 to 2 % (at most); the discrepancy in expected STE wave heights  $\zeta$  reduces from 12 to 4 % (at most). We also notice that discrepancies in standard deviations of STE do not change significantly. It is assumed, hence, that a more accurate choice of the wind forcing can lead to more accurate STE estimates than those obtained in this test case.

The approximations introduced in the implementation are only responsible for a minor effect on STE. This can be observed by comparing WW3 estimates in Table 5 with estimates obtained without approximations, i.e., using the theoretical STE model and the WW3 spectrum (Table 6). The effect of removing approximations is to improve predictions (5 % difference from observations, at most, for  $\xi$ ; 10 % difference, at most, for  $\zeta$ ) but less than what is achieved by using the observed spectrum.

**Table 6** Dimensionless STE at AA tower (March 10th 2014, 10.00UTC) estimated using (i) WW3 implementation and WASS directional spectrum, (ii) theoretical STE model and WW3 directional spectrum. Results over regions  $V_1$  ( $X = Y = 11.2$  m,  $D = 1800$  s) and  $V_2$  ( $X = Y = 30.6$  m,  $D = 450$  s). Only results for STE that have been observed (i.e.,  $\xi$  and  $\zeta$ ) are shown here

		$\xi$		$\zeta$	
		Mean	std	Mean	std
(i)	$V_1$	1.35	0.10	1.99	0.13
	$V_2$	1.39	0.10	2.04	0.13
(ii)	$V_1$	1.31	0.10	1.87	0.13
	$V_2$	1.34	0.10	1.91	0.13

WW3 underestimates the observed dimensionless STE because the direct effect of  $H_s$  on STE is removed by using dimensionless STE, but the effect of wave parameters has direct consequences on the average number of waves. For WW3  $N_V$ ,  $N_S$ , and  $N_P$  are smaller than for WASS, and this in turn reflects on smaller modeled than observed dimensionless STE. However, even if differences in wave parameters are sometimes significant (e.g., for  $\alpha_{xt}$ ,  $\alpha_{yt}$  and  $\alpha_{xy}$ ) the effect on STE is not of the same extent, but reduced, as shown by Barbariol et al. (2015). The situation is different when dimensional variables are considered, because the 20 % error on  $H_s$  estimate is added: as the model  $H_s$  is larger than the observed one, dimensional model estimates are larger than the observations.

Model-observation discrepancies of dimensionless STE wave height (12 % at most) are larger than those of the STE crest height (7 % at most). Indeed, in Eq. 12, the 4 % error on  $\psi^*$  (fully ascribed to the spectrum estimate by the model) is combined with the error committed in the estimate of the linear STE crest height. Therefore, generally, assuming a proper model representation of the wave parameters (e.g., through accurate wind forcing and appropriate model setup), the estimate of STE crest height is expected to be more accurate than that of the STE wave heights.

Showing results on two different space-time regions offers the opportunity of testing the model performance on different spatio-temporal domains. Also, it is useful to further discuss how much the STE estimate is affected by the approximations introduced in the model implementation. For instance, the use of Eq. 16 in evaluating the mode of the distribution. Indeed, through Eq. 16, the mode is a function of  $N_V$ . Hence, over  $V_2$ , where the area  $XY \approx L_x L_y$  and the average number of waves that gives the largest contribution to STE is  $N_V$ , the error introduced by the approximate solution is only 1 %. Instead, over  $V_1$ , the area  $XY \ll L_x L_y$ , and Eq. 16 underestimates the mode of 2.4 % with respect to the exact solution of  $(N_V z_1^2 + N_S z_1 + N_P) \exp(-z_1^2/2) = 1$ , since the contribution of the average number of waves  $N_S$  is comparable to that of  $N_V$ . Over the domains of analysis of this study, we can assess the effect on the STE (dimensionless) estimate of this approximation to contribute to 1 to 2 points of the discrepancies found (e.g.,  $\xi$  difference from observations over  $V_1$  would be 5 %, instead of 7 %, see Table 6). However, it is expected that this effect becomes negligible when larger areas (the model grid size, for instance) are considered.

The WW3 STE model shows better performance in simulating dimensionless STE over  $V_2$  than over  $V_1$ . However, it is worth noting that during the experiment, observed STE over  $V_1$  and  $V_2$  have been obtained using two different methods. Indeed, over  $V_1$ , STE have been observed under the condition that  $\xi > 1.25$  (i.e., one of the freak

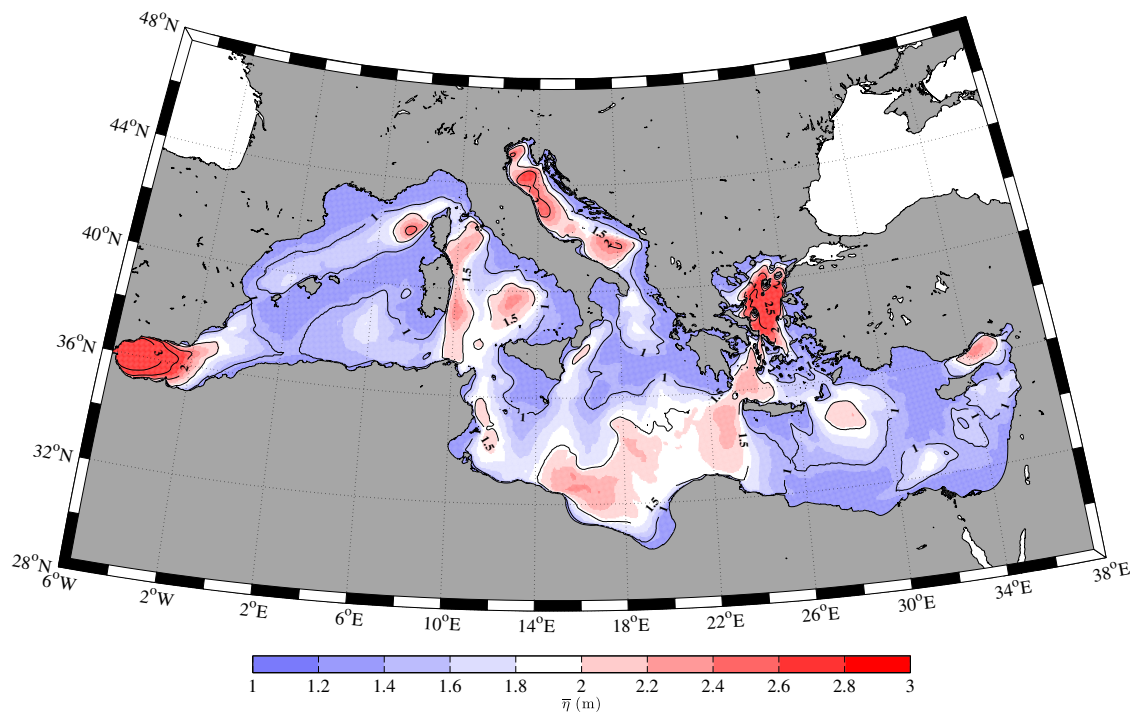


**Fig. 8** Expected dimensional STE crest height  $\bar{\eta}$  over the Mediterranean Sea on March 10th, 2014, 10.00UTC for the volume  $V_2$  ( $X = Y = 30.6$  m,  $D = 450$  s). Significant wave height (m) is depicted for reference as *black contour lines* (0.5 m spacing)

wave definitions); hence, there is a sort of conditioning on the choice of the observation time and space. On the contrary, over  $V_2$ , there is no a-priori conditioning for the choice and STE have been chosen with the only requirement of being the maximum elevations over space and time. This is the reason for the larger variability of the observations over  $V_2$ , even with a smaller number of elements (16 instead of 23). As a corollary, it is not proper to compare model-observation discrepancies over  $V_1$  with those over  $V_2$ . However, showing both of them allows to infer at the same time the performance of the model while compared to potential freak wave events (over  $V_1$ ), or to general STE without additional labels (over  $V_2$ ).

Spectral shapes (over frequency and over direction) modeled by WW3 have been found to be in fair agreement with observations, despite the differences related mainly to the wind forcing inaccuracy during the experiment. However, leaving aside the external forcing effects, we point out the opportunity of deepening the knowledge of the model effects (e.g., the wave-wave nonlinear interaction modeling) on the directional spectrum shape, and in turn on the STE. Indeed, preliminary analytical studies with a JONSWAP spectrum (Hasselmann et al. 1973) combined with a  $\cos^{2s}$  directional distribution (with  $s = 1$ ) have shown that a 5 % error on the spectral bandwidth  $\nu$  leads to a 2 % error on the STE crest height. Similar considerations hold for the error on the directional spreading which can affect the STE estimate.

Finally, the map of the expected dimensional STE crest height over the Mediterranean Sea at the time of the WASS experiment (Fig. 8) illustrates, on the one hand, that the STE estimate produced by the novel implementation of WW3 is a continuous field over space, and on the other hand that such implementation allows for large-scale prediction of wave extremes which could be useful for guidance in marine operations once a proper verification of the novel implementation will be completed. In the near future, further experiments and model runs in different met-ocean conditions and locations are planned in order to complement the dataset herein presented and provide a more comprehensive assessment of the novel implementation performance. Results from our study are a first step toward a more thorough analysis of model-observation discrepancies and behavior, which, as new observations will become available, may improve the prediction of wave STE within a numerical weather prediction framework.

**Acknowledgments** The research was partially supported by NCEP/NOAA, and partially by the Flagship Project RITMARE-The Italian Research for the Sea, coordinated by the Italian National Research Council and funded by the Italian Ministry of Education, University and Research within the National Research Program 2011-2015. Part of the research was done during the visit of Francesco Barbariol to NCEP/NOAA, supported by the 2015 Short-Term Mobility Program of the Italian National Research Council (CNR). Authors gratefully acknowledge prof. Francesco Fedele (GATECH, USA) for discussions, and CNMCA (Italy) for providing the wind model data. The WASS software is available at [www.dais.unive.it/wass/](http://www.dais.unive.it/wass/).

## References

- Adler RJ (1981) The geometry of random fields. Wiley, Chichester
- Adler RJ, Taylor JE (2007) Random fields and geometry, vol 115. Springer, New York
- Ardhuin F, Rogers E, Babanin AV, Filipot JF, Magne R, Roland A, van der Westhuysen A, Queffelec P, Lefevre JM, Aouf L, Collard F (2010) Semiempirical dissipation source functions for ocean waves. Part I: definition, calibration, and validation. *J Phys Oceanogr* 40(9):1917–1941. doi:10.1175/2010JPO4324.1.0907.4240
- Barbariol F, Benetazzo A, Bergamasco F, Carniel S, Sclavo M (2014) Stochastic space-time extremes of wind sea states: validation and modeling. In: ASME (ed) Proceedings of the 33th ASME international conference on offshore mechanics and arctic engineering (OMAE), san francisco (USA)
- Barbariol F, Benetazzo A, Carniel S, Sclavo M (2015) Space-time wave extremes: The role of metocean forcings. *J Phys Oceanogr* 45(7):1897–1916. doi:10.1175/JPO-D-14-0232.1
- Battjes J, Janssen J (1978) Energy loss and set-up due to breaking of random waves. Proceedings of the 16th international conference on coastal engineering 1(1):569–587. doi:10.9753/icce.v16. http://journals.tdl.org/icce/index.php/icce/article/view/3294
- Baxevani A, Rychlik I (2006) Maxima for Gaussian seas. *Ocean Eng* 33:895–911
- Benetazzo A, Fedele F, Gallego G, Shih PC, Yezzi A (2012) Offshore stereo measurements of gravity waves. *Coast Eng* 64:127–138
- Benetazzo A, Barbariol F, Bergamasco F, Torsello A, Carniel S, Sclavo M (2015) Observation of extreme sea waves in a space-time ensemble. *J Phys Oceanogr* 45(9):2261–2275. doi: 10.1175/JPO-D-15-0017.1
- Bertotti L, Cavaleri L, Loffredo L, Torrisi L (2013) Nettuno: analysis of a wind and wave forecast system for the mediterranean sea. *Mon Weather Rev* 141(9):3130–3141. doi: 10.1175/MWR-D-12-00361.1
- Bocchetti P (2000) Wave mechanics for ocean engineering, vol 64. Elsevier Science
- Booij N, Ris RC, Holthuijsen LH (1999) A third-generation wave model for coastal regions. I: model description and validation. *J Geophys Res* 104(C4):7649–7666
- Cavaleri L, Bertotti L (2004) Accuracy of the modelled wind and wave fields in 56A:167–175
- Cavaleri L, Barbariol F, Benetazzo A, Bertotti L, Bidlot J-R, Janssen P, Wedi N (2016a) The Draupner wave: a fresh look and the emerging view. *J Geophys Res - Oceans* 121:6061–6075
- Cavaleri L., Benetazzo A., Barbariol F., Bidlot J., Janssen P. (2016b) The Draupner event: the large wave and the emerging view. *Bull Amer Meteor Soc*:1. doi:10.1175/BAMS-D-15-00300
- Didenkulova II, Slunyaev AV, Pelinovsky EN, Kharif C (2006) Freak waves in 2005. *Nat Hazards Earth Syst Sci* 6(6):1007–1015. doi:10.5194/nhess-6-1007-2006
- Dysthe K, Krogstad HE, Müller P (2008) Oceanic rogue waves. *Annu Rev Fluid Mech* 40:287–310
- Fedele F (2012) Space-time extremes in short-crested storm seas. *J Phys Oceanogr* 42(9):1601–1615
- Fedele F (2015) On oceanic rogue waves. arXiv:1501.03370v5
- Fedele F, Tayfun MA (2009) On nonlinear wave groups and crest statistics. *J Fluid Mech* 620:221–239
- Fedele F, Benetazzo A, Gallego G, Shih PC, Yezzi A, Barbariol F, Ardhuin F (2013) Space-time measurements of oceanic sea states. *Ocean Model* 70:103–115
- Forristall G (2007) Wave crest heights and deck damage in hurricanes Ivan, Katrina and Rita. In: Offshore Technology Conference. Offshore Technology Conference, Houston, TX, USA
- Forristall GZ (2006) Maximum wave heights over an area and the air gap problem. In: Proceedings of ASME 25th Inter. Conf. Off. Mech. Arc. Eng. ASME, Hamburg, Germany, pp 11–15. OMAE2006-92022
- Gemmrich J, Garrett C (2008) Unexpected waves. *J Phys Oceanogr* 38(10):2330–2336
- Gumbel EJ (1958) Statistics of extremes. Columbia University press, New York
- Hashimoto N, Nagai T, Asai T (1994) Extension of the maximum entropy principle method for directional wave spectrum estimation. In: Proceedings of the 24th int. Conf. on coastal engineering, vol 1. ASCE, Kobe (Japan), pp 232–246
- Hasselmann K, Barnett TP, Bouws E, Carlson H, Cartwright DE, Enke K, Ewing JA, Gienapp H, Hasselmann DE, Kruseman, P, et al. (1973) Measurements of wind-wave growth and swell decay during the Joint North Sea Wave Project (JONSWAP)
- Hasselmann S, Hasselmann K, Allender JH, Barnett TP (1985) Computations and parameterizations of the nonlinear energy transfer in a gravity-wave spectrum. Part II: parameterizations of the nonlinear energy transfer for application in wave models. *J Phys Oceanogr* 15(11):1378–1391
- Janssen PAEM (2003) Nonlinear four-wave interactions and freak waves. *J Phys Oceanogr* 33(4):863–884
- Kharif C, Pelinovsky E (2003) Physical mechanisms of the rogue wave phenomenon. *Eur J Mech, B/Fluids* 22(6):603–634. doi:10.1016/j.euromechflu.2003.09.002
- Krogstad HE, Liu J, Socquet-Juglard H, Dysthe KB, Trulsen K (2004) Spatial extreme value analysis of nonlinear simulations of random surface waves. In: Proceedings of the ASME 2004 23rd International Conference on Ocean. Offshore and Arctic Engineering, ASME, Vancouver, BC, Canada
- Kuik A, Van Vledder GP, Holthuijsen LH (1988) A method for the routine analysis of pitch-and-roll buoy wave data. *J Phys Oceanogr* 18:1020–1034
- Mardia KV, Jupp PE (2009) Directional statistics. Wiley Series in Probability and Statistics, Wiley. <https://books.google.it/books?id=PTNiCm4Q-MOC>
- Onorato M, Osborne AR, Serio M, Bertone S (2001) Freak waves in random oceanic sea states. *Phys Rev Lett* 86(25):5831
- Piterbarg VI (1996) Asymptotic methods in the theory of gaussian processes and fields. AMS Transl. Math Monographs 148:206
- Sclavo M, Barbariol F, Bergamasco F, Carniel S, Benetazzo A (2015) Italian seas wave extremes: a preliminary assessment. *Rendiconti Lincei* 26(1):25–35. doi:10.1007/s12210-015-0380-y
- Signell RP, Carniel S, Cavaleri L, Chiggiato J, Doyle JD, Pullen J, Sclavo M (2005) Assessment of wind quality for oceanographic modelling in semi-enclosed basins. *J Mar Syst* 53(1):217–233
- Socquet-Juglard H, Dysthe K, Trulsen K, Krogstad HE, Liu J (2005) Probability distributions of surface gravity waves during spectral changes. *J Fluid Mech* 542(1):195–216
- Steppler J, Doms G, Schättler U, Bitzer HW, Gassmann A, Damrath U, Gregoric G (2003) Meso-gamma scale forecasts using the nonhydrostatic model {LM}. *Meteorog Atmos Phys* 82(1):75–96
- Tayfun MA (1980) Narrow-Band Nonlinear sea waves. *J Geophys Res* 85(C3):1548–1552
- Tayfun MA (2006) Statistics of nonlinear wave crests and groups. *Ocean Eng* 33:1589–1622. doi:10.1016/j.oceaneng.2005.10.007
- Tayfun MA, Fedele F (2007) Wave-height distributions and nonlinear effects. *Ocean Eng* 34:1631–1649
- The WAVEWATCH III<sup>®</sup> Development Group WW3DG (2016). User manual and system documentation of WAVEWATCH III<sup>®</sup> version 5.16. Tech. Note 329, NOAA/NWS/NCEP/MMAB, College Park, MD, USA, 326 pp. + Appendices
- Tolman HL (1991) A Third-Generation model for wind waves on slowly varying, unsteady, and inhomogeneous depths and currents. *J Phys Oceanogr* 21(6):782–797